Modeling the self-organized phosphatidylinositol lipid signaling system in chemotactic cells using quantitative image analysis

Tatsuo Shibata[1,2,3,*], Masatoshi Nishikawa[1,3], Satomi Matsuoka[3,4] and Masahiro Ueda[3,4,5]

[1]Laboratories for Physical Biology, RIKEN Center for Developmental Biology, 2-2-3 Minatojima-minamimachi, Chuo-ku, Kobe 650-0047, Japan
[2]PRESTO, Japan Science and Technology Agency (JST), 4-1-8 Honcho Kawaguchi, Saitama, Japan
[3]Japan Science and Technology Agency (JST), CREST, 1-3 Yamadaoka, Suita, Osaka 565-0871, Japan
[4]Laboratory for Cell Signaling Dynamics, RIKEN Quantitative Biology Center, 6-2-3 Furuedai, Suita, Osaka, 565-0874, Japan
[5]Laboratories for Nanobiology, Graduate School of Frontier Biosciences, Osaka University, 1-3 Yamadaoka, Suita, Osaka 565-0871, Japan
*Author for correspondence (tatsuoshibata@cdb.riken.jp)

Accepted 11 July 2012
Journal of Cell Science 125, 5138–5150

doi: 10.1242/jcs.108373

Summary

A key signaling event that is responsible for gradient sensing in eukaryotic cell chemotaxis is a phosphatidylinositol (PtdIns) lipid reaction system. The self-organization activity of this PtdIns lipid system induces an inherent polarity, even in the absence of an external chemoattractant gradient, by producing a localized PtdIns (3,4,5)-trisphosphate [PtdIns(3,4,5)P_3]-enriched domain on the membrane. Experimentally, we found that such a domain could exhibit two types of behavior: (1) it could be persistent and travel on the membrane, or (2) be stochastic and transient. Taking advantage of the simultaneous visualization of PtdIns(3,4,5)P_3 and the enzyme phosphatase and tensin homolog (PTEN), for which PtdIns(3,4,5)P_3 is a substrate, we statistically demonstrated the inter-dependence of their spatiotemporal dynamics. On the basis of this statistical analysis, we developed a theoretical model for the self-organization of PtdIns lipid signaling that can accurately reproduce both persistent and transient domain formation; these types of formations can be explained by the oscillatory and excitability properties of the system, respectively.

Key words: Cell asymmetry, Excitability, Oscillation, Spontaneous polarization

Introduction

The polarity and asymmetry of cells are important properties in diverse processes; these properties can either be induced by an extracellular cue or can be produced spontaneously. Chemotactic cells are systems in which cells form polarity and sense an extracellular chemoattractant gradient to produce a directional motion (Swaney et al., 2010). In eukaryotic chemotactic cells, such as *Dictyostelium*, a key signaling event that is responsible for directional cell migration in response to a cAMP gradient is a phosphatidylinositol (PtdIns) lipid system (Janetopoulos and Firtel, 2008; Van Haastert and Devreotes, 2004). Along a cAMP gradient, phosphoinositide 3-kinase (PI3K) catalyzes the production of PtdIns(3,4,5)P_3 from PtdIns(4,5)P_2 at the membrane region subjected to a higher cAMP concentration, while phosphatase and tensin homolog (PTEN) catalyzes the reverse reaction in the membrane region that is subjected to a lower cAMP concentration. As a result, there is an accumulation of PtdIns(3,4,5)P_3 that induces actin polymerization and leads to the formation of a pseudopod in the region of higher cAMP concentration, and, subsequently, to chemotaxis. However, accumulation of the key signaling mediator can be induced even in the absence of a cAMP gradient, as evidenced by the fact that *Dictyostelium* cells exhibit random cell migration by activating the same motility apparatus (Sasaki et al., 2007; Takagi et al., 2008). To explain the random cell migration, it would be expected that some intracellular signals spontaneously polarize. We recently found that the PtdIns lipid system is responsible for the spontaneous signal generation that promotes the random cell migration (Arai et al., 2010). In the absence of an external gradient, the PtdIns lipid system can self-organize to produce a PtdIns(3,4,5)P_3-enriched domain on the membrane in a polarized manner. In the domain, the PTEN level is reduced. The domain exhibits a variety of spatiotemporal dynamics, ranging from traveling pulses to standing waves that can last for more than 30 min. Thus, cell polarization and random cell migration can be viewed as inherent properties that are induced by the self-organizing activity of the signaling system.

Previously, self-organized activities have been observed during studies on cell motility. Vicker and colleagues found that the dynamics of cell shape include wave-like motion and oscillatory behaviors (Killich et al., 1993; Vicker, 2000). Intracellular self-organization has also been reported in *Dictyostelium* and mammalian cells, including the following: waves of actin nucleation (Gerisch et al., 2004; Weiner et al., 2007), formation of localized PtdIns(3,4,5)P_3 domains under an uniform chemoattractant stimulus (Postma et al., 2004; Postma et al., 2003) and in the absence of external cues (Weiger et al., 2009), and

Journal of Cell Science

waves of both PtdIns(3,4,5)P_3 and actin (Asano et al., 2008). More recently, a PTEN wave has also been reported (Gerisch et al., 2011).

Several theoretical models that involve self-organizing behaviors have been proposed on the basis of nonlinear mechanisms of wave generation (Meinhardt, 1999), bistability (Beta et al., 2008) and excitability (Xiong et al., 2010; Hecht et al., 2010). Although each of these models captures some of the behaviors of the PtdIns signaling system, it has been difficult to consistently explain the variety of spatiotemporal dynamics that is observed under isotropic conditions, such as formation of persistent traveling domains and formation of transient domains (Arai et al., 2010; Postma et al., 2004; Postma et al., 2003). In this paper, taking advantage of the simultaneous visualization of PtdIns(3,4,5)P_3 and its phosphatase, PTEN, in single cells, along with correlation analysis of their fluctuations, the spatial and temporal relationships between PtdIns(3,4,5)P_3 and PTEN activities are revealed. We further demonstrate the dependence of their temporal dynamics on the membrane levels of PtdIns(3,4,5)P_3 and PTEN. On the basis of these statistical analyses of our experimental data combined with known molecular biology, we present a theoretical model that accounts for self-organized signal generation. By changing parameter values, we show that the model exhibits a variety of self-organized behaviors, such as formation of persistent traveling domains of high PtdIns(3,4,5)P_3 concentration and formation of stochastic transient domains. These behaviors can be explained by the oscillatory and excitable properties of the system. By controlling the conditions experimentally, we report that the PtdIns lipid reaction system can also lead to the formation of both persistent and transient localized PtdIns(3,4,5)P_3 domains. Thus, our theoretical model captures several behaviors that are observed experimentally in the PtdIns lipid signaling system.

Results

Self-organized phosphatidylinositol signaling system

We experimentally observed the spontaneous activity in the PtdIns lipid signaling system by monitoring the level of PtdIns(3,4,5)P_3 and PTEN simultaneously on a cell membrane (Fig. 1A, see Materials and Methods). As described previously (Arai et al., 2010), cells were treated with an actin polymerization inhibitor (5 μM latrunculin A) to avoid the effects of motile and protrusive activities of the actin cytoskeleton on the PtdIns lipid signaling system. Cells were also treated with 4 mM caffeine to inhibit cell-to-cell interactions via secreted cAMP. The levels of PtdIns(3,4,5)P_3 and PTEN were monitored using the EGFP-labeled PH domain of Akt/PKB ($PH_{Akt/PKB}$–EGFP) and TMR-labeled PTEN (PTEN–TMR), respectively. As shown in Fig. 1B,C, even in the absence of a cAMP gradient and motile activities, localized PtdIns(3,4,5)P_3 and PTEN domains formed on the membrane spontaneously. Moreover, these domains were not stationary in time but traveled for at least 30 min (Arai et al., 2010). In Fig. 1B,C (center top), the time series of the levels of PtdIns(3,4,5)P_3 and PTEN (green and red, respectively) at a given position averaged over 10 pixels is plotted against time and exhibits an oscillatory behavior with a characteristic period of ~2–3 min. In Fig. 1B,C (center bottom), the two intensities are plotted as a scatter diagram (blue), showing that they have a reciprocal relationship.

Temporal correlation between PtdIns(3,4,5)P_3 and PTEN

To reveal the mechanism underlying the self-organized behavior, we first statistically characterized the temporal properties of the two fluorescence intensities. First, we evaluated the temporal behavior of PtdIns(3,4,5)P_3 levels by computing the auto-correlation function between the intensities at two time points with a time lag t at the same membrane position, $C_{PIP3}(t)$ (Fig. 2Aa, green solid line, see Materials and Methods for computation). We also computed the auto-correlation function for PTEN, $C_{PTEN}(t)$ (Fig. 2Ba, red line). Both auto-correlation functions indicated oscillatory behaviors with periods of ~3 min.

To assess how these oscillatory activities of PTEN and its substrate relate to each other temporally, we computed the cross-correlation function between the PtdIns(3,4,5)P_3 level and the PTEN membrane activity with a time lag t at the same membrane position, denoted by $C_{PIP3\text{-}PTEN}(t)$ (Fig. 2Aa, red line, see Material and Methods for computation). The cross-correlation showed the minimum value when the time delay was zero, indicating that the two intensities change temporally in an anti-correlated manner.

For a given PtdIns(3,4,5)P_3 level at a given time, consider the changes in PtdIns(3,4,5)P_3 and PTEN at a time with a time lag $t>0$. The correlation coefficients between their values at different times give the auto-correlation function $C_{PIP3}(t)$ and the cross-correlation function $C_{PIP3\text{-}PTEN}(t)$, respectively. Therefore, by comparing the two correlation functions, we obtain information on the relative timing of their temporal changes. In Fig. 2A, the first peak of $C_{PIP3\text{-}PTEN}(t)$ (red arrowhead) at ~105 sec was a positive value, indicating a positive correlation between the PtdIns(3,4,5)P_3 and PTEN levels, with a time delay of ~105 sec, whereas the first (negative) peak $C_{PIP3}(t)$ (green arrowhead) was at ~90 sec and was a negative value, indicating an anti-correlation between the PtdIns(3,4,5)P_3 level at two time points with a time lag of ~90 sec, which is half of the period. The discrepancy in the timings of the two peaks, which is ~15 sec, indicates that, for the same PtdIns(3,4,5)P_3 level at a given time, the subsequent change in the PtdIns(3,4,5)P_3 level precedes the change in the PTEN level in an anti-correlated manner. In Fig. 2B, the same timing discrepancy was also identified by comparing the auto-correlation function of PTEN, $C_{PTEN}(t)$ (red line) and the cross-correlation function between the PTEN membrane activity and the PtdIns(3,4,5)P_3 level with a time lag t at the same membrane position, denoted by $C_{PTEN\text{-}PIP3}(t)$ (green line). The first (negative) peak of $C_{PTEN}(t)$ (red open arrowhead), at ~90 sec, indicates an anti-correlation between the levels of PTEN with a time lag of ~90 sec, which is half of the period, whereas the first peak of $C_{PTEN\text{-}PIP3}(t)$ (green open arrowhead), at ~75 sec, indicates a positive correlation between the PTEN and PtdIns(3,4,5)P_3 levels, with a time delay of ~75 sec. Thus, for the same PTEN level at a given time, the subsequent change in the PTEN level follows the change in the PtdIns(3,4,5)P_3 level in an anti-correlated manner. These results demonstrate that the oscillatory PTEN activities and its substrate are correlated with a specific relative timing. The same relationship in the relative timing was also found in many cells treated with caffeine as well as latrunculin A (Fig. 2Ab,Bb, $n=52$). Considering that PTEN is the phosphatase of PtdIns(3,4,5)P_3, this order of timing is counterintuitive because the increases and decreases in the PtdIns(3,4,5)P_3 levels are expected to follow the decreases and increases of the PTEN membrane activity in the context of a simple relationship between a phosphatase and its substrate, respectively.

Spatiotemporal dynamics of PtdIns(3,4,5)P_3 and PTEN

The PtdIns(3,4,5)P_3 and PTEN levels also change spatially. As shown in Fig. 1B,C (right panels), the spatiotemporal

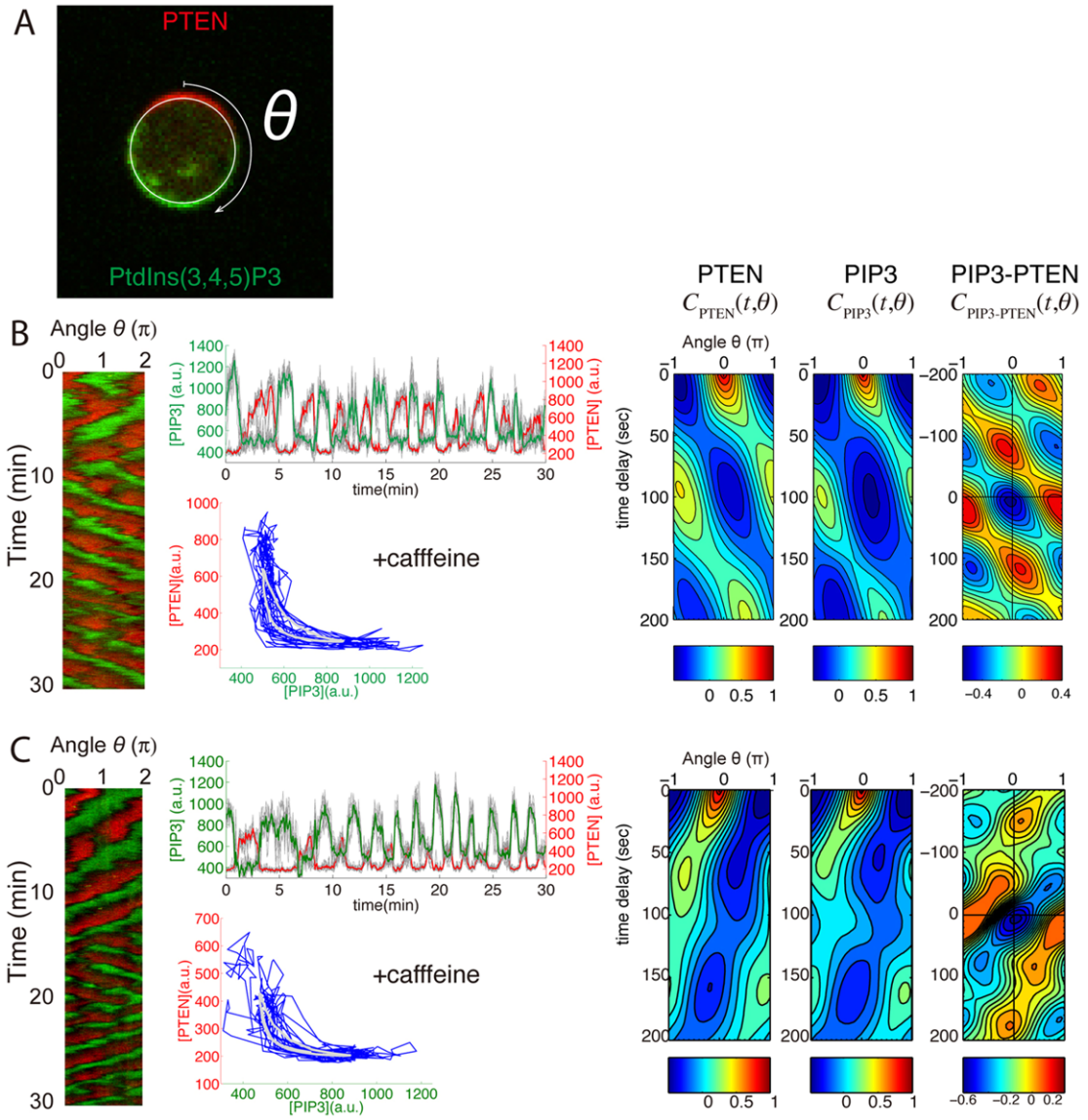

Fig. 1. Self-organization of the PtdIns signaling reaction. (**A**) Fluorescent image of a *Dictyostelium discoideum* cell expressing PTEN–TMR (red) and $PH_{Akt/PKB}$–EGFP (green). The spatial coordinate θ (0 to 2π) along the membrane. (**B**,**C**) The spatiotemporal dynamics of PtdIns signaling in cells treated with 4 mM caffeine (left). The intensities of PTEN–TMR and $PH_{Akt/PKB}$–EGFP along the membrane plotted with the angle θ and time t. Each of B and C corresponds to different single cells. Center top: The time series of the intensities of $PH_{Akt/PKB}$–EGFP and PTEN–TMR, denoted by [PIP3] and [PTEN], plotted with time. The green and red lines are obtained by averaging over the time series of successive 10 pixels at specific spatial points on the membrane (gray). Center bottom: the green and red lines shown in the top panel plotted in the [PIP3]–[PTEN] space. The gray line is the average dynamics. Right: the spatiotemporal auto-correlation functions (indicated as PTEN and PIP3) and the cross-correlation function (indicated as PIP3-PTEN).

auto-correlation functions of the two intensities showed a single peak in spatial (angle) coordinate, which indicates that a single domain is present most of the time. In the cross-correlation function in Fig. 1B,C (right panels), when the time delay was zero, the negative and positive correlations between two intensities at spatial delays $\theta=0$ and π, respectively, moved in a specific direction over time, propagating a spatial pattern. The average spatial and temporal dynamics were then extracted, as shown in supplementary material Fig. S1: the average intensities exhibited an asymmetric distribution at the peak intensities because the distribution manifested propagation in a specific direction. In this case, the direction was from 0 to π.

Extracting the average temporal dynamics of the self-organized phosphatidylinositol signaling reaction

To more precisely determine the relative dynamics between the activities of PTEN and its substrate, we extracted the average temporal behavior (average dynamics) in a cell. We first defined a phase of oscillation for a time series at a given position and time using principal components analysis (see Materials and Methods). These time series were then aligned according to the phase of oscillation of individual time series and were averaged at each aligned time point. The average time series obtained in this manner is plotted in Fig. 2Ca. From the average dynamics, we see that the local state on the plasma membrane showed

repeated transitions between the two states: in one state (open triangle), the PtdIns(3,4,5)P_3 and PTEN levels are high and low, respectively; in the other state (filled triangle), the levels are low and high, respectively. In the first state, the PTEN level reached a plateau around the minimum value until ~80 sec (red open triangle), whereas the PtdIns(3,4,5)P_3 level had already started decreasing at ~60 sec (green open triangle). When the PtdIns(3,4,5)P_3 level was near the lowest level, starting from ~125 sec (green filled triangle), the PTEN level still increased until ~170 sec (red filled triangle). The same characteristics in the relative timing of change in the intensities were also found in many cells (Fig. 2Cb, $n=52$). Therefore, in addition to the specific temporal correlation, as shown in Fig. 2A,B, the average dynamics indicated that increases and decreases of the intensities also exhibited specific timings: the increase and decrease in the level of the enzyme follows the decrease and increase in the level

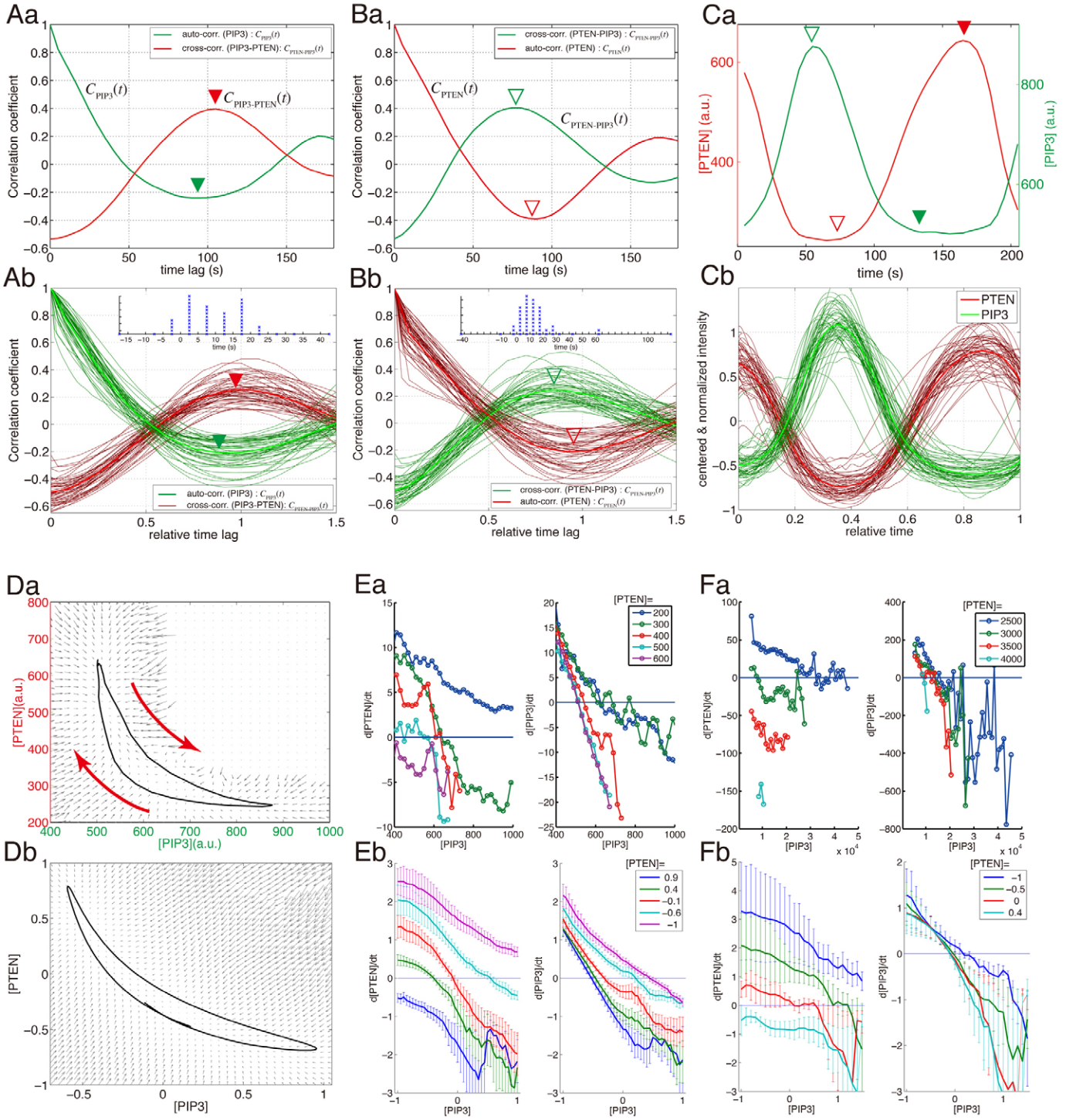

Fig. 2. See next page for legend.

of its substrate with a time delay. We have reported previously that almost all cells exhibited such time delays of 14.44±9.19 sec (n=75 cells) (see supplementary figure 4 in Arai et al., 2010). In Fig. 2D, the average dynamics are plotted in two-dimensional space, in which the two intensities changed along a crescent shape in a clockwise direction with the characteristics of the relaxation oscillator. Altogether, the reconstructed average dynamics again demonstrated that the relationship between PTEN and PtdIns(3,4,5)P_3 cannot be explained in the context of a simple phosphatase and its substrate.

The temporal changes in PtdIns(3,4,5)P_3 and PTEN intensities depend on their intensities

We next assessed the temporal behavior of [PIP3] and [PTEN], that is, the tendencies as to whether [PIP3] and [PTEN] are each increasing or decreasing when [PIP3] and [PTEN] are particular values. First, we calculated the changes in the two intensities per second, $\frac{\Delta[\mathrm{PIP3}]}{\Delta t}$ and $\frac{\Delta[\mathrm{PTEN}]}{\Delta t}$, for all of the time points and positions. By taking their averages within a range of individual values of [PIP3] and [PTEN], we then obtained the rates of change over time as functions of [PIP3] and [PTEN], denoted by $\overline{\frac{\Delta[\mathrm{PIP3}]}{\Delta t}}=f([\mathrm{PIP3}],[\mathrm{PTEN}])$ and $\overline{\frac{\Delta[\mathrm{PTEN}]}{\Delta t}}=g([\mathrm{PIP3}],[\mathrm{PTEN}])$, respectively.

As shown in Fig. 2Ea (left), for a smaller value of [PIP3], the rate of change in [PTEN], g, is positive, indicating that [PTEN] tends to increase, whereas a negative rate for a larger value of [PIP3] indicates that [PTEN] tends to decrease. For a given PTEN level, the rate of change in [PTEN] decreases almost monotonically with [PIP3], implying that g([PIP3],[PTEN]) is a decreasing function of [PIP3], which crosses zero once, from positive to negative rates. The same characteristic was also found by averaging over the population of cells as shown in Fig. 2Eb (left, n=52). Because PTEN is shuttling between the plasma membrane and the cytoplasm, this analysis indicates that the lower the PtdIns(3,4,5)P_3 level becomes, the more PTEN associates with the plasma membrane.

For PtdIns(3,4,5)P_3, a positive feedback mediated by actin polymerization has been proposed (Sasaki et al., 2007). To determine whether such a positive feedback effect is found in this case, in Fig. 2Ea (right), the rate of change in [PIP3] was plotted against [PIP3]. If a positive feedback mechanism for PtdIns(3,4,5)P_3 without affecting PTEN can be present, then the rate of change in [PIP3] would give a range of [PIP3] in which the rate increases with [PIP3]. However, the rate of change in [PIP3] decreases almost monotonically with [PIP3]. The rates of changes also averaged as decreasing functions of [PIP3] as shown in Fig. 2Eb (right, n=52). These results imply that such a feedback mechanism does not occur for this self-organization in the absence of an actin cytoskeleton.

Theoretical model of the self-organization of phosphatidylinositol lipid reactions constrained by experimental observations

On the basis of these results, we introduced a model in which the PTEN reaction depends on the level of PtdIns(3,4,5)P_3 (Fig. 3). In the previous report (Arai et al., 2010), the inhibition or deletion of PI3K and PTEN activities resulted in the disappearance of the self-organization phenomena, indicating that enzymatic activities of PI3K and PTEN are essential (Fig. 3). We consider that the enzymatic reactions are of the Michaelis–Menten type and do not have any cooperativity without any strong nonlinearity. Because these reactions are parts of the complicated phosphatidylinositol lipid reaction network (Di Paolo and De Camilli, 2006), the reactions between PtdIns(4,5)P_2 and PtdIns(3,4,5)P_3 are not isolated, and the total concentrations of both lipids can change with time. Thus, the supply and degradation of PtdIns(4,5)P_2 and PtdIns(3,4,5)P_3, independent of PI3K and PTEN, are also essential. Therefore, considering a PTEN-independent supply reaction for PtdIns(4,5)P_2 (Huang et al., 2003; Funamoto et al., 2002; Iijima and Devreotes, 2002) and PI3K- and PTEN-independent degradation pathways for PtdIns(4,5)P_2 (Korthol et al., 2007) and PtdIns(3,4,5)P_3 (Huang et al., 2003), respectively, the reaction scheme is given by the following:

$$\xrightarrow{k}\ \mathrm{PtdIns(4,5)}P_2,$$

$$\mathrm{PtdIns(4,5)}P_2 \xrightarrow{V_{\mathrm{PI3K}}\frac{[\mathrm{PIP2}]}{K_{\mathrm{PI3K}}+[\mathrm{PIP2}]}} \mathrm{PtdIns(3,4,5)}P_3,$$

$$\mathrm{PtdIns(3,4,5)}P_3 \xrightarrow{V_{\mathrm{PTEN}}[\mathrm{PTEN}]\frac{[\mathrm{PIP3}]}{K_{\mathrm{PTEN}}+[\mathrm{PIP3}]}}$$

$$\mathrm{PtdIns(4,5)}P_2,\mathrm{PtdIns(4,5)}P_2 \xrightarrow{\lambda_{\mathrm{PIP2}}[\mathrm{PIP2}]},$$

$$\mathrm{PtdIns(3,4,5)}P_3 \xrightarrow{\lambda_{\mathrm{PIP3}}[\mathrm{PIP3}]}$$

Fig. 2. Statistical analysis of the self-organization in the PtdIns signaling reaction. (**A**) The auto-correlation functions of [PIP3] (green), $C_{\mathrm{PIP3}}(t)$, and the cross-correlation function between [PIP3] and [PTEN] with a time delay t, $C_{\mathrm{PIP3\text{-}PTEN}}(t)$, (red) for the cell shown in Fig. 1B (Aa) and the population of cells (n=52, Ab). The time interval of individual cells that $C_{\mathrm{PIP3\text{-}PTEN}}(t)$ reaches the maximum value after $C_{\mathrm{PIP3}}(t)$ shows the minimum value is shown (inset). (**B**) The auto-correlation functions of [PTEN] (red), $C_{\mathrm{PTEN}}(t)$, and the cross-correlation function between [PTEN] and [PIP3] with a time delay t, $C_{\mathrm{PTEN\text{-}PIP3}}(t)$, (green) for the cell shown in Fig. 1B (Ba) and the population of cells (N=52, Bb). (**Ab,Bb**) Because the time constant of oscillation is different among cells, the time lag is normalized so that $C_{\mathrm{PIP3}}(t)$ reaches the first minimum value at time 1. The first minimum time in $C_{\mathrm{PIP3}}(t)$ averaged 115±52 seconds (±s.d.). The average correlation functions are plotted by thick lines, while the correlation functions of individual cells are shown by thin lines to show the variations. The time interval of individual cells that $C_{\mathrm{PTEN}}(t)$ reaches the maximum value after $C_{\mathrm{PTEN\text{-}PIP3}}(t)$ shows the minimum value is shown (inset). (**C**) The average dynamics of [PIP3] (green) and [PTEN] (red), plotted with time for the cell shown in Fig. 1B (Ca) and the population of cells (Cb, n=52). (Cb) The intensities of individual cells are centered and normalized. The time unit is given by the period of oscillation in individual cells [158.7 sec ± 69.4 (s.d.)]. The thick lines indicate the averages. (**D**) The average dynamics of [PIP3] and [PTEN], shown in (**C**), plotted in the [PIP3]-[PTEN] space. The gray arrows indicate the vectors of the rates of change per unit time in the two levels at [PIP3] and [PTEN], {f([PIP3],[PTEN]),g([PIP3],[PTEN])}. Because the two intensities change along these vectors, the vector field gives the dynamics out of the average dynamics. The directions of the vectors are toward the average dynamics, indicating that the average dynamics is a sink or an attractor. (**E**,**F**) For the experimental observations shown in Fig. 1B (Ea) and Fig. 5A (Fa), the rates of change per unit time in [PTEN] (left) and [PIP3] (right) are plotted against [PIP3] for a given [PTEN], as indicated in the figure. (**Eb** and **Fb**) The same rates of changes are plotted for the population of cells (n=52 (Eb) and n=10 (Fb)). As in (Cb), the intensities and the time unit are normalized. The errors show the standard error of the mean.

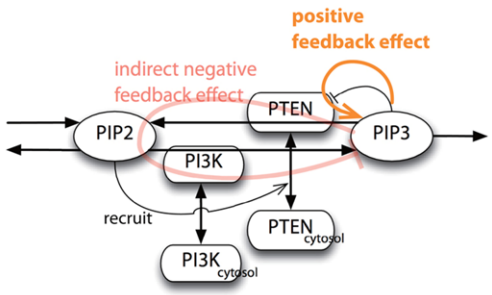

Fig. 3. A diagram of the self-organized PtdIns lipids reaction. See text for details.

where k, V_{PTEN}, K_{PTEN}, K_{PI3K}, λ_{PIP2} and λ_{PIP3} are reaction constants, V_{PI3K} is the total activity of PI3K on the membrane, including its concentration and reaction rate, and [PIP3], [PIP2], and [PTEN] are the membrane concentrations of PtdIns(3,4,5)P_3, PtdIns(4,5)P_2, and PTEN, respectively. We also consider the diffusion effect for PtdIns(4,5)P_2 and PtdIns(3,4,5)P_3 with the same diffusion constant D_{PIP}, and for PTEN with the diffusion constant D_{PTEN}.

In the model, the PTEN concentration is a variable, while the PI3K concentration is assumed to be uniform and constant along the membrane, according to our observation (Arai et al., 2010). When considering the kinetics of the membrane PTEN activity, because PTEN has a PtdIns(4,5)P_2-binding domain, we first suppose that the PTEN membrane binding rate increases with the PtdIns(4,5)P_2 concentration (Iijima et al., 2004; Campbell et al., 2003). The above statistical analysis demonstrated a possibility that PTEN associates more frequently with the membrane region with low PtdIns(3,4,5)P_3 concentration (Fig. 2E, left). Thus, we consider that the membrane binding rate of PTEN depends on the PtdIns(3,4,5)P_3 membrane concentration. The reaction scheme between the cytosol PTEN ($PTEN_{cytosol}$) and the membrane PTEN ($PTEN_{membrane}$) is then given by the following:

$$PTEN_{cytosol} \xrightarrow{V_{ass}[PTEN_{cytosol}]\frac{K_{PIP3}}{K_{PIP3}+[PIP3]}\frac{[PIP2]}{K_{PIP2}+[PIP2]}} PTEN_{membrane}$$

$$PTEN_{membrane} \xrightarrow{\lambda_{PTEN}[PTEN]} PTEN_{cytosol}$$

where, V_{ass}, K_{PIP3}, K_{PIP2} and λ_{PTEN} are reaction parameters, and $[PTEN_{cytosol}]$ is the cytosol PTEN concentration. We also evaluated a scenario in which the unbinding rate of PTEN depends on the PtdIns(3,4,5)P_3 membrane concentration, which can also explain our image data analysis. Even for such a case, we obtained almost the same results. Such dependencies have been suggested previously (Arai et al., 2010; Li et al., 2005; Papakonstanti et al., 2007; Meili et al., 2005), although their molecular basis has yet to be demonstrated.

The diffusion in the cytosol is much faster than on the membrane. Thus, the PTEN concentration in the cytosol is considered to be uniform. In this case, the PTEN concentration is given by $[PTEN_{cytosol}] = [PTEN_{total}] - \chi\overline{[PTEN]}$, where $[PTEN_{total}]$ is the total PTEN concentration, $\overline{[PTEN]}$ is the average membrane PTEN concentration and χ is the constant used to change the membrane concentration to the cytosol concentration. From a mathematical point of view, this scenario introduces a global coupling effect on the model. The fast diffusion in the cytosol can be considered to coordinate signaling reactions at individual local regions on the membrane.

Two types of behaviors were observed in the stochastic numerical simulation

We performed stochastic numerical simulations for the scheme shown in the theoretical model described above (see Materials and Methods). As shown in Fig. 4A, the PtdIns(3,4,5)P_3 domain formed persistently and traveled along the membrane, reproducing the experimental observation (Fig. 1B,C). The stochastic noise induced a domain disappearance and a reversal of the traveling direction, producing a spatiotemporal variability in the pattern dynamics. In Fig. 4A (right), for the simulation data, we performed the statistical analysis that was applied to the experimental data (Fig. 2D) to obtain the average dynamics, which, on average, exhibited a similar characteristic crescent-shape dynamics, and the trajectories rotated in the clockwise direction, as is the case for the experiment.

In addition to the traveling waves, the model exhibited another type of spatiotemporal dynamics when parameter values were changed. In Fig. 4B,C, we changed the parameter values, such as the maximum rate of the PI3K total enzymatic activity, V_{PI3K} (Fig. 4B), and the degradation rate of PtdIns(4,5)P_2, λ_{PIP2} (Fig. 4C). As a result, the PtdIns(3,4,5)P_3 domain became

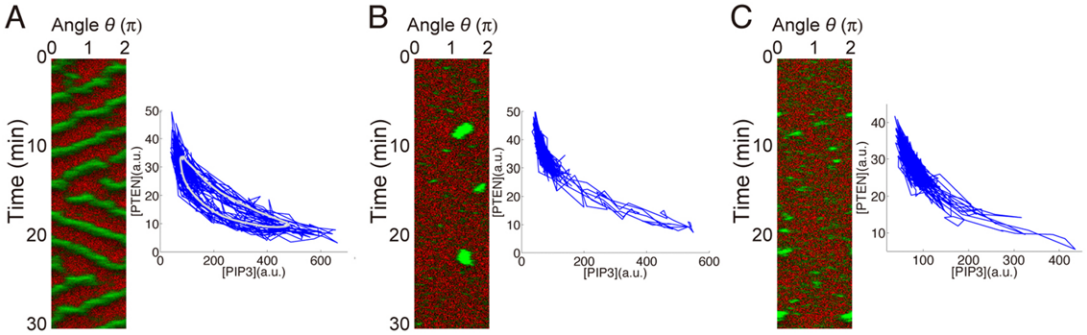

Fig. 4. Spatiotemporal plot of [PIP3] (green) and [PTEN] (red) (left panel) and the trajectory of two values at a specific spatial point plotted in the [PIP3] and [PTEN] space (right), obtained numerically starting from random initial conditions for the systems with the following parameters: (**A**) V_{PI3K}=600 molecules μm^{-2} s^{-1}, λ_{PIP2}=0.002 s^{-1}. (**B**) V_{PI3K}=470 molecules μm^{-2} s^{-1}, λ_{PIP2}=0.005 s^{-1}. (**C**) V_{PI3K}=560 molecules μm^{-2} s^{-1}, λ_{PIP2}=0.01 s^{-1}, and (**A**–**C**) k=45 molecules μm^{-2}s^{-1}, V_{PTEN}=15s^{-1}, K_{PTEN}=50 molecules μm^{-2}, K_{PI3K}=3500 molecules μm^{-2}, λ_{PIP3}=0.2 s^{-1}, V_{ass}=1300 molecules μm^{-2} μM^{-1}s^{-1}, K_{PIP3}=120 molecules μm^{-2}, K_{PIP2}=3000 molecules μm^{-2}, D=0.2 μm^2 s^{-1}, D_{PTEN}=0.15 μm^2 s^{-1} , λ_{PTEN}=1 s^{-1}, $[PTEN_{total}]$=0.1 μM, and χ=10^{-3} μM μm^2 molecules^{-1}.

transient, and the formation of domains took place randomly in time and space. This domain formation probably resulted from the stochastic reaction noise triggering a large excursion of PtdIns(3,4,5)P_3 levels (Fig. 4B,C, right), leading to a transient formation of the domain. When the domain formed, the level of PTEN was reduced. Thus, the levels of the two factors are anti-correlated.

Experimental observation of two types of behaviors

As we reported previously, caffeine treatment might play a role in not only inhibiting cell-to-cell interactions but also stabilizing the formation of the PtdIns(3,4,5)P_3 domain (Arai et al., 2010). Thus, we investigated the spatiotemporal dynamics of the PtdIns lipids reaction system in the absence of caffeine and with low cell density to avoid cell-to-cell interactions (Materials and Methods). As shown in Fig. 5, the PtdIns(3,4,5)P_3 domains formed transiently and appeared randomly (Tsai et al., 2008; Postma et al., 2004; Postma et al., 2003; Xiong et al., 2010). In Fig. 5 (right), the spatiotemporal auto-correlation functions of the PTEN and PtdIns(3,4,5)P_3 levels indicated that the correlation at $t=0$ and $\theta=0$ decayed in less than 50 seconds and typically in ~10 seconds, without spatial propagation. The cross-correlation functions demonstrated the anti-correlation between the PtdIns(3,4,5)P_3 and PTEN levels, as in the numerical results (Fig. 4B,C, right).

To further determine whether the transient formation of the domain observed experimentally is consistent with our theoretical model, we statistically analyzed the time series. We assessed the rates of change in [PIP3] and [PTEN], denoted by $\overline{\frac{\Delta[\mathrm{PIP3}]}{\Delta t}}=f([\mathrm{PIP3}],[\mathrm{PTEN}])$ and $\overline{\frac{\Delta[\mathrm{PTEN}]}{\Delta t}}=g([\mathrm{PIP3}],[\mathrm{PTEN}])$, respectively. For a given level of PTEN, the rates of change in [PIP3] and [PTEN] decrease almost monotonically with [PIP3] (Fig. 2Fa), as in the case of persistent domain formation (Fig. 2E). The rate of change averaged over population of cells ($n=10$) are shown in Fig. 2Fb, and have the same characteristic. These results indicate the consistency between the experimental observation and the model.

Thus, our theoretical model can reproduce both types of spatiotemporal dynamics observed experimentally: namely, persistent and transient formations of domains. Removing caffeine probably alters some of the biochemical parameters in the PtdIns lipids signaling system (see Discussion).

The system exhibits both oscillatory and excitable behaviors

How can a single model explain both persistent and transient domain formation? To explore this question, we first evaluated the properties of the local reaction without taking into account diffusion effects and reaction noise (Eqns 1–4 in Materials and Methods). We show that the two types of behaviors are related to the oscillatory and excitable properties that are exhibited by the PtdIns lipids reaction system.

Because PTEN is responsible for the degradation of PtdIns(3,4,5)P_3, we noted that the reciprocal dependence of PTEN membrane localization on PtdIns(3,4,5)P_3 level can have a positive effect on the production of PtdIns(3,4,5)P_3 (Fig. 3). However, because a decrease in the membrane PTEN concentration also results in a reduction of PtdIns(4,5)P_2 production, which then reduces the production rate of PtdIns(3,4,5)P_3, an indirect negative effect can be present for the production of PtdIns(3,4,5)P_3. Thus, the PtdIns lipid reaction system consists of a combination of fast positive- and slow negative-feedback loops for PtdIns(3,4,5)P_3. Such double-feedback loops are known to be capable of being responsible for both oscillation and excitability. Thus, our result that the rate of change in [PTEN] was a decreasing function of [PIP3] (Fig. 2E), indicates an essential mechanism for the excitation and oscillation dynamics.

First, we demonstrate that our model for the PtdIns lipids signaling system shows excitability. Compared with [PIP3] and [PTEN], [PIP2] is much larger and changes at a slower rate. Thus, for short time scales, [PIP2] can be considered constant while [PIP3] and [PTEN] change. For evaluating a local reaction, the cytosol PTEN concentration was fixed. The temporal evolution of [PIP3] and [PTEN] (i.e. the trajectory) were obtained through model equations using conditions where [PIP2] was constant and started from several initial states (Fig. 6A). Because the direction of the trajectory changes on the nullclines given by d[PIP3]/dt=0 and d[PTEN]/dt=0 (red and green), the behaviors of the trajectory can be inferred from these nullclines. The intersections of the two lines give the fixed points. In Fig. 6A, point **a** gives the resting state that corresponds to the low [PIP3] state, while point **c** gives the excited state, which corresponds to the high [PIP3] state. The line through the unstable fixed point **b**, indicated by gray, is called the separatrix. If the state is not beyond the separatrix after a perturbation is applied to the resting state **a**, the trajectory returns to **a**. If the state is beyond the separatrix, the trajectory moves away from **a** and reaches the excited state **c** with a high [PIP3]. Thus, the separatrix provides a threshold to reach the other state.

To observe the behavior of the system when the state approaches the excited state **c** beyond the separatrix, it is necessary to take into account the change in [PIP2] for a slow time scale. As the state reaches the excited state c, [PIP2] starts to change gradually, which leads to a shift in the nullclines, as indicated in Fig. 6B. As a result of the shift, both the excited state **c** and the unstable fixed point **b** disappear, and only the resting state **a** remains. Consequently, the state returns to the resting state **a,** with low [PIP3]. After [PIP2] returns to the stationary state, the system can be excitable for the next perturbation (Fig. 6A).

The temporal evolutions of [PIP3], [PIP2] and [PTEN] obtained using Eqn 4 induced by different initial perturbations are projected on the [PIP3]–[PTEN] space (Fig. 6C). As expected from Fig. 6A, when a perturbation shifts the state over the threshold, the trajectory reaches the excited state. Then, as indicated in Fig. 6B, the state returns to the resting state (filled circle in Fig. 6C). This type of behavior in the PtdIns signaling system is a characteristic of excitable systems. A perturbation necessary for the excitation may be caused by the transient production of PtdIns(3,4,5)P_3 by PI3K, which is induced stochastically, or by a cAMP stimulus that leads to an increase in [PIP3]. Reaction noises also play important roles for the spontaneous formation of a PtdIns(3,4,5)P_3 domain.

This model for the PtdIns lipids system can also exhibit repeated excitation. Such an oscillatory behavior is possible if the production of PtdIns(3,4,5)P_3 is always larger than a threshold value. When the total PI3K enzymatic activity, V_{PI3K}, is larger than a critical value, and the cytosol PTEN concentration [$\mathrm{PTEN}_{\mathrm{cytosol}}$] is set to be an appropriate constant value, the resting state **a** and the unstable fixed point **b** disappear, as shown in Fig. 6D. As a result, the trajectory moves to the excited state **c**,

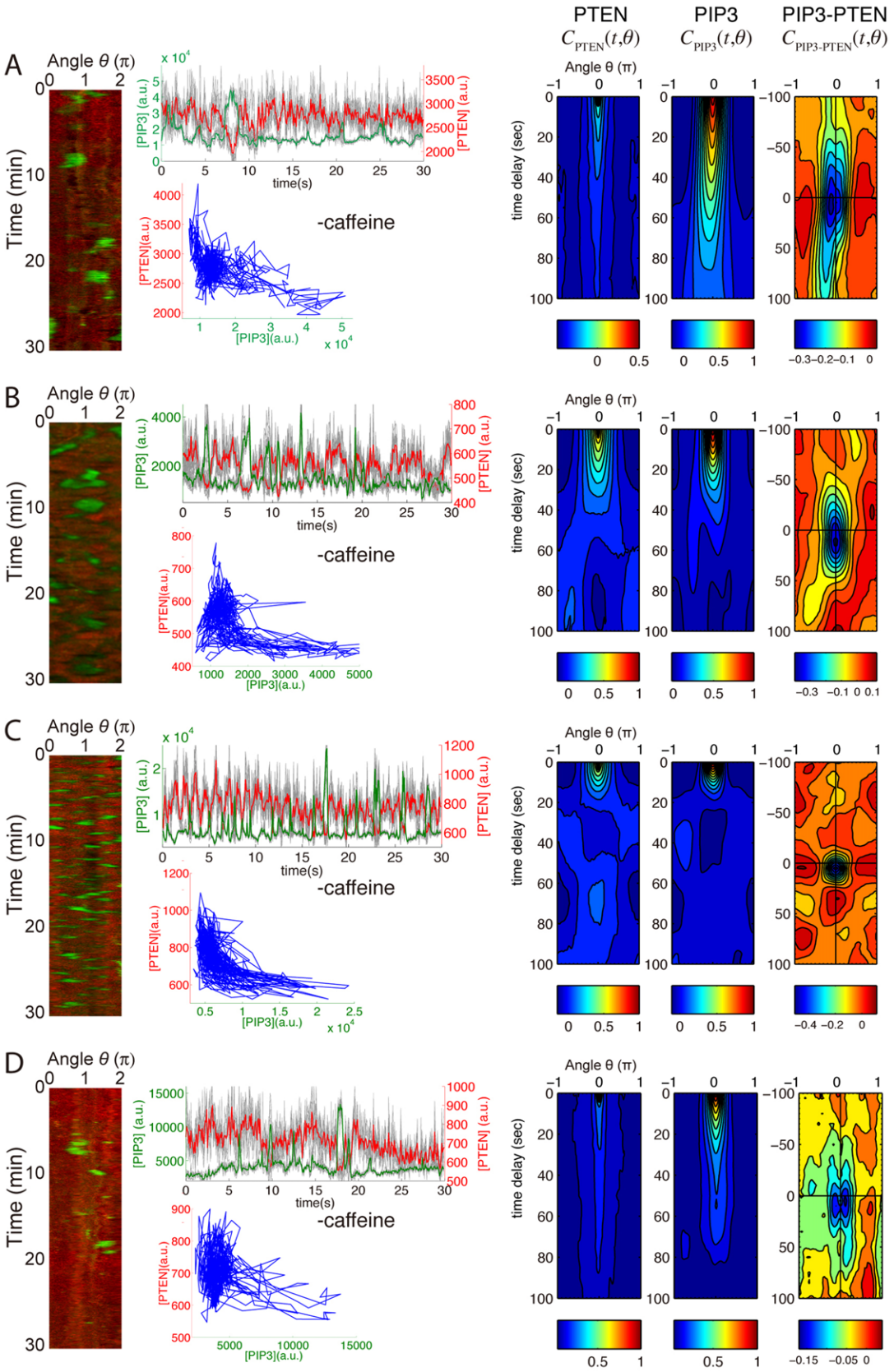

Fig. 5. Spontaneous PtdIns(3,4,5)P_3-enriched domain formation in cells without caffeine treatment. (**A–D**) Each plot corresponds to four different single cells. Left: gallery of space-time plot of the intensities of PTEN–TMR and $PH_{Akt/PKB}$–EGFP along the cell membrane. Center top: the time series of the intensities. Center bottom: the scatter diagram of the time series, and (right) the spatiotemporal correlation functions. See legend to Fig. 1 for details.

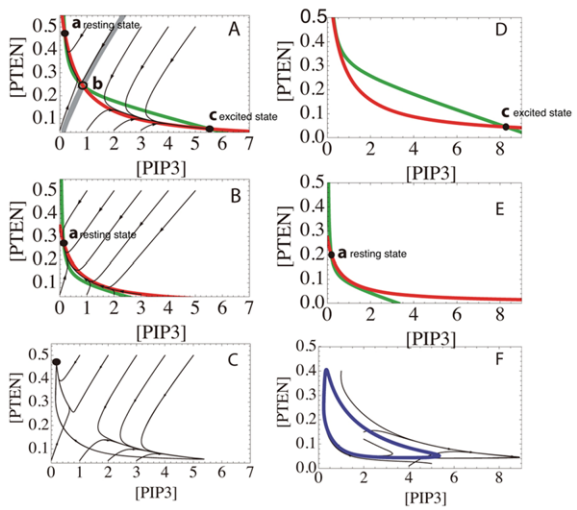

Fig. 6. Mechanism of excitability and oscillation in the PtdIns signaling reaction. (**A**–**C**) The excitable case. (A) Nullclines (red and green lines), and the trajectories (black lines) are plotted. The gray line is the separatrix. [PIP2] in Eqn. 4 is set to be the stationary value (y=163.5). (B) [PIP2] was reduced by 150 from the stationary value. (C) Trajectories induced by different initial perturbations projected on the [PIP3]–[PTEN] space. (**D**–**F**) The oscillation case. Here, we used $\bar{z}$=0.233, which was obtained from Fig. 7E. (D) Nullclines plotted by red and green lines. [PIP2] in Eqn 4 is y=40. (E) [PIP2] in Eqn 4 is y=5. (F) Trajectories projected on the [PIP3]-[PTEN] space. Here, the non-dimensional equation without the diffusion term in Eqn 4 was used. The parameter values are given by v_1=33.3, K_1=0.22, K_2=15.5, v_0=6.5, K_4=0.53, K_5=13.3, and λ=5, λ_y=0.005. (A–C) v_2=8. (D–F) v_2=13.5.

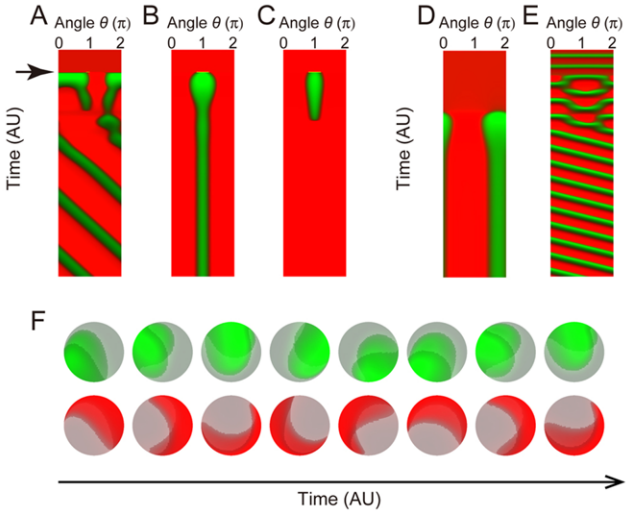

Fig. 7. A variety of spatiotemporal dynamics of the PtdIns lipids signaling system. (**A**–**C**) The stationary state is stable. A perturbation is applied at the time indicated by the arrow. A sufficiently large perturbation is applied in a small area. (A) A traveling domain is produced; v_1=33.3 and v_2=10. (B) A stationary domain is produced; v_1=33.3 and v_2=8.5. (C) A stationary domain is produced transiently; v_1=33.3 and v_2=8. (**D**,**E**) The stationary state is unstable. (D) A stationary domain is spontaneously formed; v_1=18 and v_2=5.77. (E) A traveling domain is spontaneously produced; v_1=33.3 and v_2=14. (**F**) The traveling spots or spiral wave formation in the two-dimensional surface of a spherical cell; v_1=33.3 and v_2=13. Here, we used the non-dimensional equations (Eqn 4). Other parameter values are given in Fig. 6.

increasing [PIP3]. Because [PIP2] also changes, the nullclines shift, which leads to the appearance of resting state **a** and, finally, to the disappearance of excited state **c**, as shown in Fig. 6E. Thus, the trajectory reaches around the excited state **c** and then starts to return toward the resting state **a**. As the system returns to resting state **a**, the nullclines shift, making the excited state **c** appear again, and the resting state **a** then disappears. This cycling between states **a** and **c** gives rise to the relaxation oscillation, which is a characteristic of the experimentally observed dynamics (Fig. 1B,C). In Fig. 6F, the trajectories obtained using Eqn 4, starting from different initial points, are projected on the [PIP3] and [PTEN] space.

It is clear that the structures of the nullclines (the red and green lines) determine the shape of the trajectories in the [PIP3] and [PTEN] space, which are similar to the experimental observations (Figs. 1, 5 and 6).

A variety of spatiotemporal dynamics

We next assessed the spatiotemporal pattern formation in which the effect of diffusion is taken into account and the cytosol PTEN concentration can be time-dependent (Eqns 1–3 and Eqn 4).

We first considered the case for which the stationary uniform state stably exists, in which all of the areas along the membrane stay in the resting state **a**. In this model, when a sufficiently large increase in [PIP3] is applied in a small local area, a local reaction can exhibit excitability. Possible spatiotemporal patterns in excitable media with diffusion effects have been studied extensively. In such medium, the perturbation can be caused by a diffusional flow from a neighboring area. As a result, the burst of PtdIns(3,4,5)P_3 can propagate to produce a traveling domain (Fig. 7A and Fig. 8A). If the traveling velocity of the domain decreases to zero for some parameter values, then a localized stationary domain could also be possible (Fig. 7B). For some parameter values, those pulses and spots might appear only transiently and might not be stable (Fig. 7C and Fig. 8B) (Arai et al., 2010; Hecht et al., 2010). The size of the domain is intrinsically determined by the balance between the excitable property of the local elements and the effect of diffusion.

The stationary uniform state becomes unstable when the PI3K activity V_{PI3K} or the PtdIns(4,5)P_2 degradation rate λ_{PIP2} exceeds a critical value. Non-uniform patterns typically grow with a spatial pattern with wave number 1, leading to the formation of spatiotemporal patterns, such as a stationary domain and a traveling domain (Fig. 7D,E and Fig. 8A). When a traveling domain is produced, the local reaction exhibits an oscillation. Such destabilization of a stationary uniform state also takes place by changing other parameter values, such as the PTEN activity (V_{PTEN}) and the total PTEN concentration [$PTEN_{total}$]. A detailed bifurcation diagram is shown in supplementary material Fig. S2.

In two-dimensional systems, a spiral wave is typically generated if a stripe-shaped travelling wave is broken at a point. A stationary and propagating spot or domain has also been studied (Krischer and Mikhailov, 1994). In the two-dimensional surface of a spherical cell (Fig. 7F), PtdIns(3,4,5)P_3 and PTEN-enriched spots were produced exclusively and travel in a direction, which were similar to spiral waves.

We note that the global coupling term derived from the diffusion through the cytosol is essential and important. A strong global coupling makes the system stable for a spatially uniform perturbation, while it is unstable for a non-uniform perturbation.

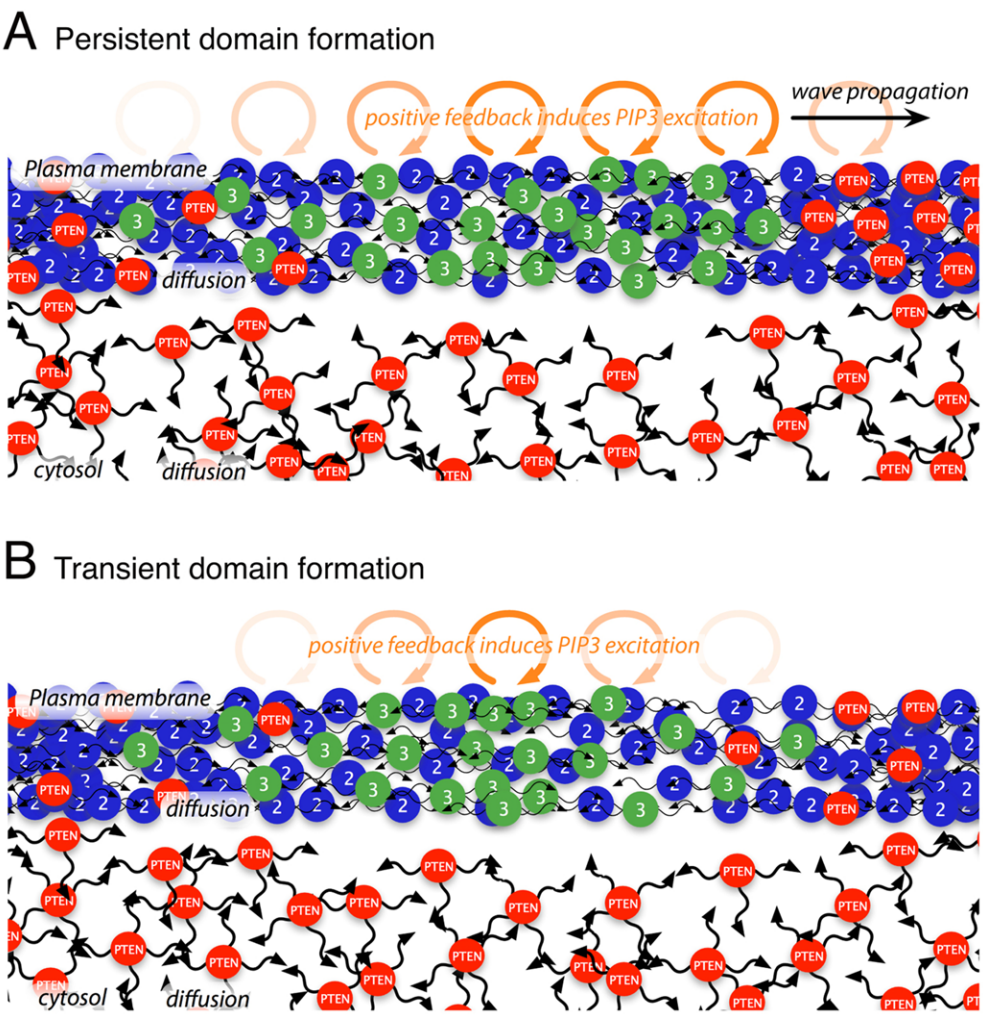

Fig. 8. The self-organization in excitable and oscillatory systems through membrane diffusion. (**A**) Persistent domain formation. Once the concentration gradient of PtdIns(3,4,5)P_3 (green) is established, the gradient drives net flux of PtdIns(3,4,5)P_3 from the enriched-domain to the lower concentration region. The flux at the front of domain triggers a PtdIns(3,4,5)P_3 burst through positive feedback, moving the boundary of the front of domain outward. At the rear of domain, the concentration of PtdIns(4,5)P_2 is decreased, which prevents the positive feedback of PtdIns(3,4,5)P_3 to work, moving the boundary inwards. Consequently, the PtdIns(3,4,5)P_3-enriched domain shows a propagation. (**B**) Transient domain formation. When a PtdIns(3,4,5)P_3-enriched domain is formed, if the diffusional flux cannot trigger a further PtdIns(3,4,5) burst in the neighboring areas, the domain is attenuated.

As a result, a non-uniform and polarized distribution can be developed easily. Moreover, in this case, the total PTEN concentration is conserved between the membrane and the cytosol. This mass conservation imposes a further regulatory effect, by which a PtdIns(3,4,5)P_3-enriched domain formation results in an increase in the cytosol PTEN concentration, leading to restriction of the further formation of domains.

Variability of spatiotemporal dynamics induced by reaction noise

Because a cell is such a small system, a large reaction noise is inevitable. Thus, inside a cell, such a reaction noise, in addition to the diffusional flow discussed above, can cause perturbations that induce bursts in the PtdIns(3,4,5)P_3 concentration (Fig. 8). Here, we performed a stochastic numerical simulation to evaluate the effect of stochasticity in reactions. When the parameter values were set within the region where the stationary uniform state is stable and the system is not excitable, PtdIns(3,4,5)P_3-accumulating domains were not produced, even in the presence of noise. When the system is in an excitable state, there are large stochastic noise-induced formations of PtdIns(3,4,5)P_3 domains (Fig. 4B,C), which is similar to the experimental observations shown in Fig. 5. The domains appear transiently and become extinct because either the stochasticity of the reaction destroys the domain or the domain is intrinsically unstable. When the stationary uniform state is unstable, patterns were spontaneously produced without an effect of the reaction noise (Fig. 7D,E). The internal noise in the reactions leads to a variability in the pattern dynamics, such as the fusion and fission of domains and a reversal in the direction of the domain propagation (Fig. 4A). Thus, depending on the parameter values, there are three types of behaviors under the isotropic condition (Fig. 8): (1) a uniform state that is stable without excitability, (2) a uniform state that is stable with excitability, and (3) a uniform state that is unstable. The two behaviors observed in our experiment (Figs 1 and 5), could correspond to the latter two behaviors of the theoretical model; treatment with caffeine could modulate some of the biochemical parameter values to change the cellular states between them.

Discussion

In this paper, we propose mathematical mechanisms that produce spontaneously an asymmetric activity of PtdIns signaling system in *Dictyostelium* cells based on statistical analysis of imaging data. The traveling wave of PtdIns(3,4,5)P_3 is induced by an instability of the stationary uniform state (Fig. 1B,C), while for the transient domain formation, noise plays an important role in triggering a PtdIns(3,4,5)P_3 burst of excitable dynamics (Fig. 5).

This self-organization in the PtdIns signaling system produces an intracellular signal that is independent of extracellular anisotropy. Such a spontaneous signal generation can be responsible for random cell motility in the absence of external cues (Postma et al., 2004; Arai et al., 2010; Postma et al., 2003). The formation of PtdIns(3,4,5)P_3-enriched domains under isotropic cAMP stimulus conditions has been reported by Postma et al. (Postma et al., 2003; Postma et al., 2004). In that case, the domain lifetime is less than a few minutes, which is comparable to our observations in the absence of caffeine treatment. These observations, together with our results, indicate that the lifetime of PtdIns(3,4,5)P_3 domains is distributed from a few tens of seconds to more than a few minutes (Fig. 5, right), which is comparable to or is larger than the lifetime of pseudopodia, which is less than a few tens of seconds. It is probable that the localized PtdIns(3,4,5)P_3 domain defines an area in which pseudopodia are produced and the frequency of pseudopodia formation is elevated. As a result, random cell migration would show a correlation with the migration direction with a time scale of approximately a few minutes (Arai et al., 2010; Takagi et al., 2008). Therefore, the localized PtdIns(3,4,5)P_3 domain can be considered to be a directional memory. Such a role for PtdIns(3,4,5)P_3-enriched domains will be experimentally validated in future studies.

In the model shown in Fig. 3, we assumed either an inhibition of membrane binding or an acceleration of membrane dissociation of PTEN by PtdIns(3,4,5)P_3 based on the results of our imaging data analysis (Fig. 2). Such dependences have been also suggested previously (Arai et al., 2010; Li et al., 2005; Papakonstanti et al., 2007; Meili et al., 2005). The molecular mechanism would require an effect of PtdIns(3,4,5)P_3 on the activity of binding sites for PTEN on the plasma membrane or PTEN itself. An increasing number of proteins have been identified that interact with PTEN on the membrane in mammalian cells including MAGI-2, P-REX2a and NHERF1/EBP50 (Wu et al., 2000; Fine et al., 2009; Molina et al., 2010). However, no binding protein for PTEN has been reported in *Dictyostelium* cells. An identification of the binding proteins for *Dictyostelium* PTEN and a characterization of the dependence of the affinity between PTEN on PtdIns(3,4,5)P_3 will provide in-depth understanding of the molecular mechanism in the self-organizing activity of PtdIns signaling system. In mammalian cells, phosphorylation of PTEN has been reported to regulate the membrane association and activity of PTEN (Rahdar et al., 2009). In contrast, little has been known about the phosphorylation of *Dictyostelium* PTEN. Our previous study demonstrated that the membrane association of constitutively dephosphorylated human PTEN was equivalent to that of *Dictyostelium* PTEN in *Dictyostelium* cells (Vazquez et al., 2006). Thus, *Dictyostelium* PTEN is considered to behave similarly to the constitutively dephosphorylated form, and the self-organization of the PtdIns signaling system still occurs under these conditions. Another mechanism would couple to the catalytic activity of PTEN onto PI(3,4,5)P_3. Several PTEN mutants could be used to discern such a mechanism, which remains to be demonstrated.

To observe the traveling wave behavior stably, we treated cells with caffeine. However, a recent report indicated that *Dictyostelium* cells without caffeine treatment also exhibit a wave of GFP–PTEN on the membrane (Gerisch et al., 2011). The period of wave reported was approximately the same with ours, indicating that the stable wave generation might not be restricted to cells with caffeine treatment. We suggested that caffeine treatment changes some of the parameter values. One possibility is that caffeine affects the activity of PI3K. We have reported that the frequency of activation of Ras is increased in the presence of caffeine (Sasaki et al., 2007; Arai et al., 2010). In contrast, it has been reported that Ras is not activated in the absence of caffeine (Sasaki et al., 2007; Sasaki et al., 2007). Ras is supposed to be necessary for the activation of PI3K (Arai et al., 2010; Sasaki et al., 2007). Thus, this scenario could explain the transition between excitable and oscillatory states of the PtdIns signaling system. Another possibility is that caffeine could affect other parameters, such as the activity of PTEN and the PtdIns(4,5)P_2 supply and degradation rates, which have effects on the stability of the stationary uniform state (supplementary material Fig. S2).

Our results demonstrated that the rate of change in the PTEN membrane concentration was anti-correlated with the PtdIns(3,4,5)P_3 intensity (Fig. 2E,F). As a result, a PtdIns(3,4,5)P_3-enriched domain is expected to be more stable with a longer lifetime. When a PtdIns(3,4,5)P_3-enriched domain is produced in the front region of a motile cell in the absence of external cues, PTEN could exhibit a reduced distribution in the region (see figure 6 in Arai et al., 2010). Furthermore, the specific timing between the changes in PtdIns(3,4,5)P_3 and PTEN concentrations, as reported in this paper, is important for self-organization, which is made possible through a mechanism of nonlinear dynamical systems. By the self-organized mechanism, stochastic reaction noises are organized to produce asymmetric distributions. The significance of the self-organization in the chemotaxis cells is that an asymmetric distribution could specify the direction as a memory, which could be controlled by an external gradient and could store its directional information. How external and internal processes, such as an extracellular gradient, could control and bias the polarized distribution of a key factor is a question to be addressed in future studies.

Materials and Methods

Cell preparation

Cell construction and growth conditions were as described previously (Arai et al., 2010). Cells were starved by suspension in development buffer (DB: 5 mM Na phosphate buffer, 2 mM $MgSO_4$, 0.2 mM $CaCl_2$, pH 6.3) for 1 hour and were then pulsed with 10 nM cAMP at 6-minute intervals for up to 3.5 hours, leading to the polarized cell shape with chemotactic competency. $PH_{Akt/PKB}$-EGFP- and PTEN-Halo-expressing cells were then treated with 5 μM tetramethylrhodamine (TMR)-labeled Halo-ligand (G8251, Promega) for 30 minutes to label PTEN with TMR in living cells. For caffeine treatment, 4 mM caffeine was added to the solution during TMR-Halo-ligand treatment. After washing out the TMR-Halo-ligand, cells were settled on a glass dish (IWAKI) at a given cell density in the presence of 5 μM latrunculin A (L5163, Sigma) and were incubated for 20 minutes. For the caffeine-untreated cells, the cell density was kept at less than 5×10^3 cells/ml to eliminate cell-to-cell interactions via secreted cAMP. For $PH_{Akt/PKB}$–EGFP expressing cells, cells were treated with 4 mM caffeine for 30 minutes after the cAMP pulsation. Cells were incubated on a glass dish in DB in the presence of 4 mM caffeine and 5 μM latrunculin A for 20 minutes.

Microscopy

Confocal imaging was performed using inverted microscopes (TiE, Nikon) equipped with a spinning disk confocal unit (CSU X1, Yokogawa). $PH_{Akt/PKB}$-EGFP and PTEN-TMR were excited by 488 and 561 nm solid-state lasers, respectively. Fluorescence images were acquired with an EMCCD camera (iXon+, Andor). Images of $PH_{Akt/PKB}$-EGFP- and PTEN-TMR-expressing cells were taken every 5 sec. Image analysis was performed using Matlab (Mathworks).

Correlation function analysis

The temporal auto-correlation functions of PtdIns(3,4,5)P_3 and PTEN are given by $C(t) = \frac{\overline{(I(0)-\mu)\cdot(I(t)-\mu)}}{\sigma^2}$ and, respectively, where $I(t)$ is the fluorescence intensity of $PH_{Akt/PKB}$–EGFP or PTEN–TMR at the same membrane position at time t, μ is the mean intensities, and σ^2 is its variances. The cross-correlation

functions are given by $C_{\mathrm{PIP3\text{-}PTEN}}(t)=\frac{\overline{(I_{\mathrm{PIP3}}(0)-\mu_{\mathrm{PIP3}})\cdot(I_{\mathrm{PTEN}}(t)-\mu_{\mathrm{PTEN}})}}{\sigma_{\mathrm{PIP3}}\sigma_{\mathrm{PTEN}}}$ and $C_{\mathrm{PTEN\text{-}PIP3}}(t)=\frac{\overline{(I_{\mathrm{PTEN}}(0)-\mu_{\mathrm{PTEN}})\cdot(I_{\mathrm{PIP3}}(t)-\mu_{\mathrm{PIP3}})}}{\sigma_{\mathrm{PIP3}}\sigma_{\mathrm{PTEN}}}$, respectively. The spatiotemporal–dimensional autocorrelation function is given as $C(\theta,t)=\frac{\overline{(I(\theta,t)-\mu)\cdot(I(0,0)-\mu)}}{\sigma^2}$, where $I(\theta,t)$ is the fluorescence intensity of $PH_{Akt/PKB}$–EGFP or PTEN–TMR at position θ along the membrane at time t. Here, μ and σ represent the mean and standard deviation of $I(\theta,t)$, respectively. The spatiotemporal cross-correlation function is given as $C_{\mathrm{PIP3-PTEN}}(\theta,t)=\frac{\overline{(I_{\mathrm{PIP3}}(0,0)-\mu_{\mathrm{PIP3}})\cdot(I_{\mathrm{PTEN}}(\theta,t)-\mu_{\mathrm{PTEN}})}}{\sqrt{\sigma^2_{\mathrm{PIP3}}}\sqrt{\sigma^2_{\mathrm{PTEN}}}}$.

Extracting the average dynamics of [PIP3] and [PTEN]

The average dynamics shown in Fig. 2C,D were extracted from the time series of the PTEN–TMR and $PH_{Akt/PKB}$–EGFP fluorescence intensities using principal components analysis (PCA). PCA was performed using $2n$ variables for the fluorescence intensities of PTEN–TMR and $PH_{Akt/PKB}$–EGFP, each with n time points (a time window) at a given position. First, the PTEN–TMR and $PH_{Akt/PKB}$–EGFP fluorescence intensities were centered and normalized (z-scores). Next, we performed PCA for data and obtained $2n$ principal components. The scores of the first two principal components ($c_1(\theta,t)$,$c_2(\theta,t)$) at position θ and time t give the phase of the oscillation, $\phi(\theta,t)$, which is defined as $c_1=r\cos\phi$,$c_2=r\sin\phi$ with $r=\sqrt{{c_1}^2+{c_2}^2}$. To obtain the average dynamics, the time of each data point was shifted by $-\phi T/2\pi$, where T is the period of oscillation. The shifted data were then averaged over the data at individual time points.

The reaction diffusion equations

For the reaction scheme shown in the main text, the spatiotemporal dynamics without the effect of stochasticity are described by the reaction diffusion equation given by the following:

$$\begin{aligned}\frac{\partial[\mathrm{PIP3}]}{\partial t}&=-R_{\mathrm{PTEN}}+R_{\mathrm{PI3K}}-\lambda_{\mathrm{PIP3}}[\mathrm{PIP3}]+D_{\mathrm{PIP}}\nabla^2[\mathrm{PIP3}]\\ \frac{\partial[\mathrm{PIP2}]}{\partial t}&=R_{\mathrm{PTEN}}-R_{\mathrm{PI3K}}+k-\lambda_{\mathrm{PIP2}}[\mathrm{PIP2}]+D_{\mathrm{PIP}}\nabla^2[\mathrm{PIP2}]\\ \frac{\partial[\mathrm{PTEN}]}{\partial t}&=V_{ass}[\mathrm{PTEN_{cytosol}}]\frac{K_{\mathrm{PIP3}}}{K_{\mathrm{PIP3}}+[\mathrm{PIP3}]}\frac{[\mathrm{PIP2}]}{K_{\mathrm{PIP2}}+[\mathrm{PIP2}]}-\lambda_{\mathrm{PTEN}}[\mathrm{PTEN}]+D_{\mathrm{PTEN}}\nabla^2[\mathrm{PTEN}]\end{aligned}\quad(1)$$

with

$$[\mathrm{PTEN_{cytosol}}]=[\mathrm{PTEN_{total}}]-\chi\overline{[\mathrm{PTEN}]}\quad(2)$$

and

$$\begin{aligned}R_{\mathrm{PI3K}}&=V_{\mathrm{PI3K}}\frac{[\mathrm{PIP2}]}{K_{\mathrm{PI3K}}+[\mathrm{PIP2}]},\\ R_{\mathrm{PTEN}}&=V_{PTEN}[\mathrm{PTEN}]\frac{[\mathrm{PIP3}]}{K_{PTEN}+[\mathrm{PIP3}]}\end{aligned}\quad(3)$$

Parameters

Because the transition between high and low concentrations of $PtdIns(3,4,5)P_3$ is essential, K_{PTEN} was set to be larger than the $PtdIns(3,4,5)P_3$ level at the resting state, while smaller than the level at the excited state. In this model, PTEN associates more frequently with the membrane region with low $PtdIns(3,4,5)P_3$ level. Thus, the parameter K_{PIP3} that defines the $PtdIns(3,4,5)P_3$ level at which the switching of the PTEN binding rate takes place is set to be the value between the two states. The $PtdIns(4,5)P_2$ concentration fluctuated around K_{PI3K} and K_{PIP2}. Both K_{PI3K} and K_{PIP2} are approximately set to the membrane $PtdIns(4,5)P_2$ concentration, which is estimated to be approximately 4000 molecules/μm^2 (Xu et al., 2003). (The population density of $PtdIns(4,5)P_2$ is estimated to be 0.5% of the total phospholipids, which is 60% of the total area of the plasma membrane.) These parameter values set the concentrations for both lipids in a range such that the $PtdIns(4,5)P_2$ concentration (approximately a few thousand molecules per μm^2) is always larger than the $PtdIns(3,4,5)P_3$ concentration (<1000 molecules per μm^2). The diffusion coefficient of PTEN is given in Vazquez et al. (Vazquez et al., 2006; see also Arai et al., 2010).

Numerical simulations

For numerical simulations, we evaluated a one-dimensional system along the membrane. The radius of the cells was chosen to be 5 μm, which is typical for latrunculin A-treated cells. For the stochastic simulation, we used the estimated-midpoint τ-leap method (Gillespie, 2001) with 100 grids and a constant time step $\Delta t=0.0005$. To obtain the concentration at each grid, the molecular numbers were divided by the grid size Δx (μm) or $1\times\Delta x$ (μm^2).

Non-dimensional equations

For the assessment of spatiotemporal dynamics without the effect of stochasticity, we use the non-dimensional reaction diffusion equation. Rescaling time, spatial coordinates and concentrations as $t\rightarrow t\lambda_{\mathrm{PIP3}}^{-1}$, $\mathbf{r}\rightarrow\mathbf{r}\sqrt{D_{\mathrm{PIP}}/\lambda_{\mathrm{PIP3}}}$, $[\mathrm{PIP3}]\rightarrow xk\lambda_{\mathrm{PIP3}}^{-1}$, $[\mathrm{PIP2}]\rightarrow yk\lambda_{\mathrm{PIP3}}^{-1}$, and considering $[\mathrm{PTEN}]\rightarrow z[\mathrm{PTEN_{total}}]/\chi$, Eqns 1–3 can be rewritten as

$$\begin{aligned}\frac{\partial x}{\partial t}&=-v_1z\frac{x}{K_1+x}+v_2\frac{y}{K_2+y}-x+\Delta x\\ \frac{\partial y}{\partial t}&=v_1z\frac{x}{K_1+x}-v_2\frac{y}{K_2+y}+1-\lambda_y y+\Delta y\\ \frac{\partial z}{\partial t}&=v_0(1-\bar{z})\frac{K_4}{K_4+x}\frac{y}{K_5+y}-\lambda z+d\Delta z\end{aligned}\quad(4)$$

where $\bar{z}$ is the instantaneous spatial average. The coefficients are $v_1=V_{\mathrm{PTEN}}[\mathrm{PTEN_{total}}]k^{-1}\chi^{-1}$, $K_1=K_{\mathrm{PTEN}}\lambda_{\mathrm{PIP3}}k^{-1}$, $v_2=V_{\mathrm{PI3K}}k^{-1}$, $K_2=K_{\mathrm{PI3K}}\lambda_{\mathrm{PIP3}}k^{-1}$, $\lambda_y=\lambda_{\mathrm{PIP2}}\lambda_{\mathrm{PIP3}}^{-1}$, $v_0=V_{ass}\chi\lambda_{\mathrm{PIP3}}^{-1}$, $K_4=K_{\mathrm{PIP3}}\lambda_{\mathrm{PIP3}}k^{-1}$, $K_5=K_{\mathrm{PIP2}}\lambda_{\mathrm{PIP3}}k^{-1}$, $\lambda=\lambda_{\mathrm{PTEN}}\lambda_{\mathrm{PIP3}}^{-1}$, and $d=D_{\mathrm{PTEN}}/D_{\mathrm{PIP}}$. The bifurcation diagram is shown in Fig. S2 for the non-dimensional parameters, v_1, v_2, and λ_y. The stationary uniform state changes its stability from stable with excitability to unstable; for example, this state change is achieved by increasing v_2, decreasing v_1 or decreasing λ_y.

Acknowledgements

We thank A. S. Mikhailov and H. Takagi for their discussions and comments on this manuscript.

Funding

This work was supported by grant-in-aid (KAKENHI) from MEXT [grant number 23111531 to T.S. and M.U.].

Supplementary material available online at
http://jcs.biologists.org/lookup/suppl/doi:10.1242/jcs.108373/-/DC1

References

Arai, Y., Shibata, T., Matsuoka, S., Sato, M. J., Yanagida, T. and Ueda, M. (2010). Self-organization of the phosphatidylinositol lipids signaling system for random cell migration. *Proc. Natl. Acad. Sci. USA* **107**, 12399-12404.

Asano, Y., Nagasaki, A. and Uyeda, T. Q. (2008). Correlated waves of actin filaments and PIP3 in Dictyostelium cells. *Cell Motil. Cytoskeleton* **65**, 923-934.

Beta, C., Amselem, G. and Bodenschatz, E. (2008). A bistable mechanism for directional sensing. *New J. Phys.* 10.

Campbell, R. B., Liu, F. and Ross, A. H. (2003). Allosteric activation of PTEN phosphatase by phosphatidylinositol 4,5-bisphosphate. *J. Biol. Chem.* **278**, 33617-33620.

Di Paolo, G. and De Camilli, P. (2006). Phosphoinositides in cell regulation and membrane dynamics. *Nature* **443**, 651-657.

Fine, B., Hodakoski, C., Koujak, S., Su, T., Saal, L. H., Maurer, M., Hopkins, B., Keniry, M., Sulis, M. L., Mense, S. et al. (2009). Activation of the PI3K pathway in cancer through inhibition of PTEN by exchange factor P-REX2a. *Science* **325**, 1261-1265.

Funamoto, S., Meili, R., Lee, S., Parry, L. and Firtel, R. A. (2002). Spatial and temporal regulation of 3-phosphoinositides by PI 3-kinase and PTEN mediates chemotaxis. *Cell* **109**, 611-623.

Gerisch, G., Bretschneider, T., Müller-Taubenberger, A., Simmeth, E., Ecke, M., Diez, S. and Anderson, K. (2004). Mobile actin clusters and traveling waves in cells recovering from actin depolymerization. *Biophys. J.* **87**, 3493-3503.

Gerisch, G., Ecke, M., Wischnewski, D. and Schroth-Diez, B. (2011). Different modes of state transitions determine pattern in the Phosphatidylinositide-Actin system. *BMC Cell Biol.* **12**, 42.

Gillespie, D. T. (2001). Approximate accelerated stochastic simulation of chemically reacting systems. *J. Chem. Phys.* **115**, 1716-1733.

Hecht, I., Kessler, D. A. and Levine, H. (2010). Transient localized patterns in noise-driven reaction-diffusion systems. *Phys. Rev. Lett.* **104**, 158301.

Huang, Y. E., Iijima, M., Parent, C. A., Funamoto, S., Firtel, R. A. and Devreotes, P. N. (2003). Receptor-mediated regulation of PI3Ks confines $PI(3,4,5)P_3$ to the leading edge of chemotaxing cells. *Mol. Biol. Cell* **14**, 1913-1922.

Iijima, M. and Devreotes, P. N. (2002). Tumor suppressor PTEN mediates sensing of chemoattractant gradients. *Cell* **109**, 599-610.

Iijima, M., Huang, Y. E., Luo, H. R., Vazquez, F. and Devreotes, P. N. (2004). Novel mechanism of PTEN regulation by its phosphatidylinositol 4,5-bisphosphate binding motif is critical for chemotaxis. *J. Biol. Chem.* **279**, 16606-16613.

Janetopoulos, C. and Firtel, R. A. (2008). Directional sensing during chemotaxis. *FEBS Lett.* **582**, 2075-2085.

Killich, T., Plath, P. J., Wei, X., Bultmann, H., Rensing, L. and Vicker, M. G. (1993). The locomotion, shape and pseudopodial dynamics of unstimulated Dictyostelium cells are not random. *J. Cell Sci.* **106**, 1005-1013.

Kortholt, A., King, J. S., Keizer-Gunnink, I., Harwood, A. J. and Van Haastert, P. J. (2007). Phospholipase C regulation of phosphatidylinositol 3,4,5-trisphosphate-mediated chemotaxis. *Mol. Biol. Cell* **18**, 4772-4779.

Krischer, K. and Mikhailov, A. (1994). Bifurcation to traveling spots in reaction-diffusion systems. *Phys. Rev. Lett.* **73**, 3165-3168.

Li, Z., Dong, X., Wang, Z., Liu, W., Deng, N., Ding, Y., Tang, L., Hla, T., Zeng, R., Li, L. et al. (2005). Regulation of PTEN by Rho small GTPases. *Nat. Cell Biol.* **7**, 399-404.

Meili, R., Sasaki, A. T. and Firtel, R. A. (2005). Rho Rocks PTEN. *Nat. Cell Biol.* **7**, 334-335.

Meinhardt, H. (1999). Orientation of chemotactic cells and growth cones: models and mechanisms. *J. Cell Sci.* **112**, 2867-2874.

Molina, J. R., Morales, F. C., Hayashi, Y., Aldape, K. D. and Georgescu, M.-M. (2010). Loss of PTEN binding adapter protein NHERF1 from plasma membrane in glioblastoma contributes to PTEN inactivation. *Cancer Res.* **70**, 6697-6703.

Papakonstanti, E. A., Ridley, A. J. and Vanhaesebroeck, B. (2007). The p110delta isoform of PI 3-kinase negatively controls RhoA and PTEN. *EMBO J.* **26**, 3050-3061.

Postma, M., Roelofs, J., Goedhart, J., Gadella, T. W., Visser, A. J. and Van Haastert, P. J. (2003). Uniform cAMP stimulation of Dictyostelium cells induces localized patches of signal transduction and pseudopodia. *Mol. Biol. Cell* **14**, 5019-5027.

Postma, M., Roelofs, J., Goedhart, J., Loovers, H. M., Visser, A. J. and Van Haastert, P. J. (2004). Sensitization of Dictyostelium chemotaxis by phosphoinositide-3-kinase-mediated self-organizing signalling patches. *J. Cell Sci.* **117**, 2925-2935.

Rahdar, M., Inoue, T., Meyer, T., Zhang, J., Vazquez, F. and Devreotes, P. N. (2009). A phosphorylation-dependent intramolecular interaction regulates the membrane association and activity of the tumor suppressor PTEN. *Proc. Natl. Acad. Sci. USA* **106**, 480-485.

Sasaki, A. T., Janetopoulos, C., Lee, S., Charest, P. G., Takeda, K., Sundheimer, L. W., Meili, R., Devreotes, P. N. and Firtel, R. A. (2007). G protein-independent Ras/PI3K/F-actin circuit regulates basic cell motility. *J. Cell Biol.* **178**, 185-191.

Swaney, K. F., Huang, C. H. and Devreotes, P. N. (2010). Eukaryotic chemotaxis: a network of signaling pathways controls motility, directional sensing, and polarity. *Annu. Rev. Biophys.* **39**, 265-289.

Takagi, H., Sato, M. J., Yanagida, T. and Ueda, M. (2008). Functional analysis of spontaneous cell movement under different physiological conditions. *PLoS ONE* **3**, e2648.

Tsai, T. Y., Choi, Y. S., Ma, W., Pomerening, J. R., Tang, C. and Ferrell, J. E. J., Jr (2008). Robust, tunable biological oscillations from interlinked positive and negative feedback loops. *Science* **321**, 126-129.

Van Haastert, P. J. and Devreotes, P. N. (2004). Chemotaxis: signalling the way forward. *Nat. Rev. Mol. Cell Biol.* **5**, 626-634.

Vazquez, F., Matsuoka, S., Sellers, W. R., Yanagida, T., Ueda, M. and Devreotes, P. N. (2006). Tumor suppressor PTEN acts through dynamic interaction with the plasma membrane. *Proc. Natl. Acad. Sci. USA* **103**, 3633-3638.

Vicker, M. G. (2000). Reaction-diffusion waves of actin filament polymerization/depolymerization in Dictyostelium pseudopodium extension and cell locomotion. *Biophys. Chem.* **84**, 87-98.

Weiger, M. C., Wang, C. C., Krajcovic, M., Melvin, A. T., Rhoden, J. J. and Haugh, J. M. (2009). Spontaneous phosphoinositide 3-kinase signaling dynamics drive spreading and random migration of fibroblasts. *J. Cell Sci.* **122**, 313-323.

Weiner, O. D., Marganski, W. A., Wu, L. F., Altschuler, S. J. and Kirschner, M. W. (2007). An actin-based wave generator organizes cell motility. *PLoS Biol.* **5**, e221.

Wu, X., Hepner, K., Castelino-Prabhu, S., Do, D., Kaye, M. B., Yuan, X. J., Wood, J., Ross, C., Sawyers, C. L. and Whang, Y. E. (2000). Evidence for regulation of the PTEN tumor suppressor by a membrane-localized multi-PDZ domain containing scaffold protein MAGI-2. *Proc. Natl. Acad. Sci. USA* **97**, 4233-4238.

Xiong, Y., Huang, C. H., Iglesias, P. A. and Devreotes, P. N. (2010). Cells navigate with a local-excitation, global-inhibition-biased excitable network. *Proc. Natl. Acad. Sci. USA* **107**, 17079-17086.

Xu, C., Watras, J. and Loew, L. M. (2003). Kinetic analysis of receptor-activated phosphoinositide turnover. *J. Cell Biol.* **161**, 779-791.